Ore Geology Reviews 166 (2024) 105933

Contents lists available at ScienceDirect

Ore Geology Reviews

journal homepage: www.elsevier.com/locate/oregeorev

Contrasting granites associated with W, Sn, and Be mineralization in the Xuebaoding and Pingwu areas, Sichuan Province, SW China

Xinxiang Zhu [a], Markus B. Raschke [b,*], Yan Liu [a,*]

[a] SinoProbe Laboratory, Institute of Geology, Chinese Academy of Geological Sciences, Beijing 100037, PR China
[b] Department of Physics, and JILA, University of Colorado, Boulder, CO 80309, USA

ARTICLE INFO

Keywords:
Highly fractionated granite
W–Sn–Be mineralization
S-type granite

ABSTRACT

Rare metals (e.g., tungsten, tin, or beryllium) are critical strategic elements mainly hosted by magmatic-hydrothermal ore deposits associated with granitic intrusions. The simultaneous occurrence of W, Sn, and Be is unusual, and the underlying processes leading to the formation of corresponding ore deposits is not yet understood. In that regard, the Xuebaoding W-Sn-Be deposit in the Songpan-Garzê Orogenic Belt of western China stands out with its exceptionally high Be content with only weak alteration. While the Xuebaoding deposit has been the subject of much previous petrographic, geochronological, mineralogical, and ore-forming fluid investigations, few studies have yet addressed the regional granitoid rocks around the deposit and their potential association with the Xuebaoding system. Here, a contrasting lithologic, geochemical, chronological, and Sr–Nd–Pb isotope analyses of granites from neighboring intrusions with only W mineralization near Pingwu is performed. The Pingwu granites are found to be S-type, of 211.4 ± 0.7 to 229.8 ± 0.6 Ma age, with high A/CNK values (>1.07), and Sr–Nd–Pb isotope values of $^{87}Sr/^{86}Sr_{(i)}$ = 0.70589–0.71486, $\varepsilon Nd_{(t)}$ = −3.49 to −9.51, $^{206}Pb/^{204}Pb$ = 17.9378–18.3996, $^{207}Pb/^{204}Pb$ = 15.5693–15.6836, and $^{208}Pb/^{204}Pb$ = 38.1382–38.7390. In addition, these granites are low in W (0.06–4.1 ppm), Sn (1.0–7.3 ppm) and Be (1.6–8.6 ppm). A comparison with the Xuebaoding granites suggests a cogenetic origin, but a lower degree of fractionation in the Pingwu system. The different petrogenesis of the W occurrences near Pingwu with respect to the W–Sn–Be deposit are likely due to a combination of protolith, melting mechanism, and ore-controlling structures. The work highlights the unusual conditions necessary for the spatial or temporal coexistence of W, Sn, and Be mineralization within the same deposit as represented by only few deposits worldwide.

1. Introduction

Tungsten, tin, and beryllium are critical strategic elements in high demand for next-generation technologies (e.g., energy applications, alloys) (Chakhmouradian et al., 2015; Trueman and Sabey, 2014; Sovacool et al., 2020). Globally, most W, Sn, and Be resources are hosted by magmatic-hydrothermal ore deposits associated with granitic intrusions (Lehmann, 1990; Linnen et al., 2012). These granites, thus designated as rare-metal granites, generally exhibit enrichment in both rare metals (e.g., W, Sn, Be, Nb, Ta, Cs, and Rb) and fluxing elements (e.g., F, B, P, and Li) together with a marked depletion in REE, Y, Ca, Fe, Ba, and Sr (Černý and Ercit, 2005; Linnen et al., 2012). Previous studies have generally attributed the W and Sn segregation to granite compositions, different degrees of partial melting and fractionation, and redox states (Blevin and Chappell, 1992, 1995; Lehmann, 2020; Zhao et al., 2022). Beryllium saturation in granitic melts was shown to require extreme fractionation and low temperatures, which is typically linked to granitic pegmatites (London, 2008, 2015).

Globally, most granite related W–Sn deposits are dominated by massive scheelite, disseminated cassiterite and skarn- and greisen-type alteration, with minor beryl (Mao et al., 2013; Mao et al., 2019; Liao et al., 2021). A deposit known for its up to decimeter size euhedral and gem quality minerals of beryl, scheelite, cassiterite, apatite, fluorite, and muscovite, with only weak alteration is that of Xuebaoding (Fig. 1; Yan et al., 2010; Cao et al., 2002, 2004; Rakovan, 2007; Li et al., 2007; Liu et al., 2007a; Liu et al., 2007b; Liu et al., 2007c; Liu et al., 2010; Zhang et al., 2014; Zhu et al., 2020; Yokart et al., 2003; Somarin and Ashley, 2004; Bettencourt et al., 2005; Pettke et al., 2005; Esmaeily et al., 2005; Macey and Harris, 2006; Neiva, 2008; Liu et al., 2012a; Liu et al., 2012b; Wang et al., 2021). It is located in the Songpan-Garzê Orogenic Belt,

* Corresponding authors.
E-mail addresses: markus.raschke@colorado.edu (M.B. Raschke), ly@cags.ac.cn (Y. Liu).

https://doi.org/10.1016/j.oregeorev.2024.105933
Received 2 September 2023; Received in revised form 9 December 2023; Accepted 2 February 2024
Available online 5 February 2024

about 5 km SE of the mountain Xuebaoding (elevation 5,588 m) and is associated with highly evolved leucogranites (Cao et al., 2002, 2004; Rakovan, 2007; Li et al., 2007; Liu et al., 2007a; Liu et al., 2007b; Liu et al., 2007c; Liu et al., 2010; Zhang et al., 2014). However, the mechanisms leading to its simultaneous mineralization of W, Sn and Be are still not well understood.

Previous studies mainly focused on formation ages, granitic petrogenesis, and ore-forming fluids of the Xuebaoding deposit (e.g., Zhang et al., 2021; Wu et al., 2017), with few studies having yet addressed the petrogenesis of other granites in the region. Most notable are a range of granite intrusions to the east of Xuebaoding, chiefly confined by the Huya fault in the west, Pingwu town to the east, and situated north of the Fujiang river. This area is known for scheelite occurrences, that have been historically mined commercially, associated with quartz, and minor apatite. In contrast to Xuebaoding, the Pingwu area system does not host cassiterite and beryl, and is not associated with muscovite.

In this study, a detailed petrographic study of granites from the Pingwu area is provided, based on field work, and geochemical and Sr–Nd–Pb isotope analyses and U–Pb ages. The results are compared with the mineralized granites of Xuebaoding in order to address similarities and distinctions relating to W and W–Sn–Be mineralization in general.

2. Geological setting

The long-term intracontinental convergence and associated series of magmatic and metamorphic events with the subsequent Himalayan movement (ca. 80 Ma) resulted in the folding of the Songpan-Ganzi orogenic belt (Xu and Li, 2013; Kirby and Ouimet, 2011). The active Huya fault system, which separates Precambrian basement and overlying late Proterozoic to Permian rock units to its east, from the Triassic Songpan-Ganzê flysch sequences to its west, contributes to the ongoing uplift of the Minshan (Kirby and Ouimet, 2011). Tectonically, the Xuebaoding area is situated in the Songpan-Ganzê orogenic belt, west of the Sichuan basis, facing the Qinling orogenic belt to the north, and the Yangtze block to the east and south-east (Fig. 1; Yan et al., 2010). The stratigraphy of the Xuebaoding area with elevation ranging from 1400 to 5588 m, consists of a series of metamorphic rock units intercalated with carbonate rocks of thickness randing from 1500 to 2000 m. Magmatic rocks are dominated by alkali granites (Fig. 1; Cao et al., 2002; Yan et al., 2010).

The Xuebaoding W–Sn–Be deposit, is on the SE side of the Little Xuebaoding mountain with mineralized areas ranging chiefly from 3800 to 4100 m in elevation, intruding along the core of a dome (Fig. 1). It is mainly composed of several Mesozoic albite granite intrusions (Pankou, Pukou, Wuzhutang etc.), locally exposed across < 100 m to ca. 1 km range, dated at 194–201 Ma coincident to the late Indosinian orogeny to early Yanshan (Ye et al., 2001; Zhou et al., 2002; Cao et al., 2004; Li et al., 2007). The stratigraphic sequence of the Xuebaoding deposit is nearly overturned, steeply dipping to the east of the granite contacts. The main mineralization occurs in factures and joints both in the Pankou and Pukouling granites as well as the hosting marble and schist (Liu

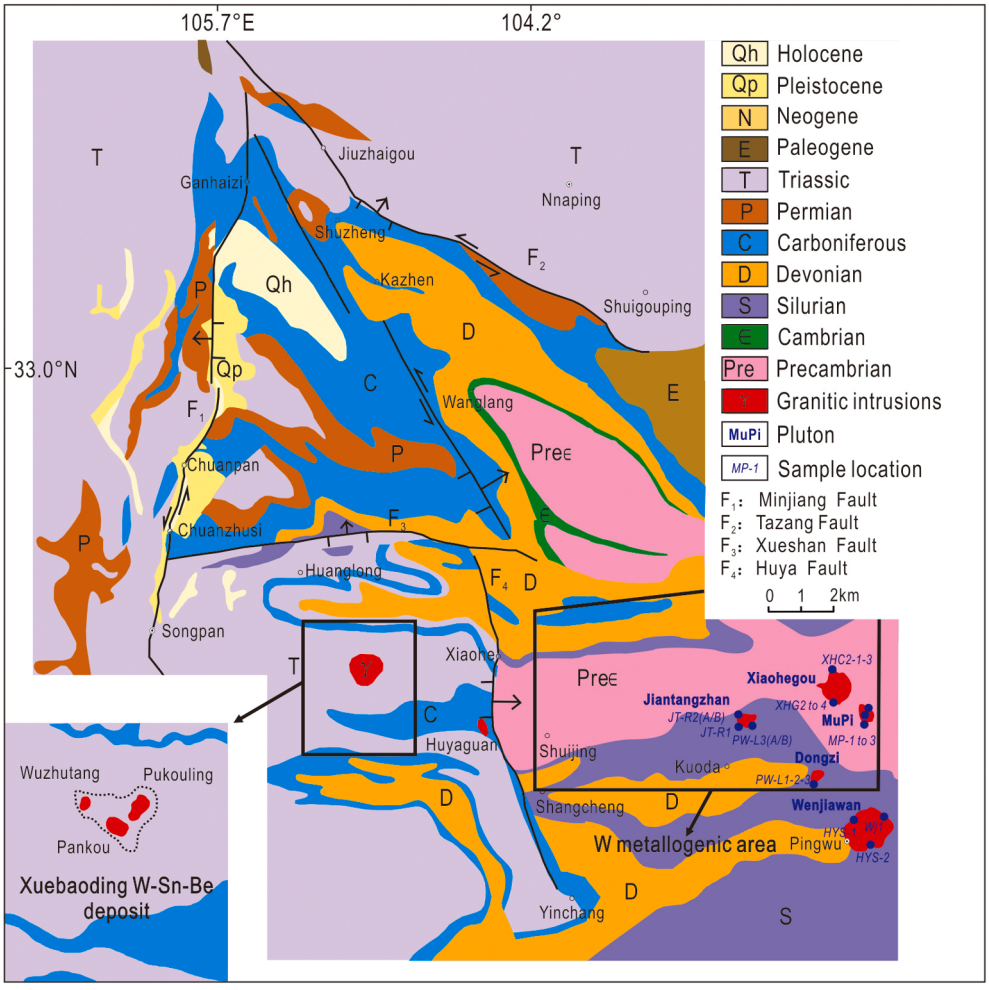

Fig. 1. Simplified geological map of the Pingwu and Xuebaoding study area, with the granitic plutons in the vicinity of the Pingwu in the general area of small scheelite W deposits. Figure modified after Liu et al., 2018.

et al., 2012b). The veins of primarily quartz, fluorite, calcite, and muscovite gauge are locally rich in beryl, cassiterite, and scheelite (Liu et al., 2010). In contrast, east of the Huya fault, the stratigraphy lacks the Carboniferous-Permian limestone and Triassic flysch, which are widely distributed on the west. The terrains on both sides of the fault are significantly undulating, with various landforms. The west side is located in the Minshan block exhibiting the higher planation surface than the east side of about 1000 m (Liu et al., 2018). Multiple magmatic intrusions and tungsten mining have been reported on the east side, but detailed information on them is relatively scarce (Fig. 1).

A large number of mineralized zones occur over an area of 10 km (north–south extent) by 30 km (east–west) with quartz and calcite veins with minor apatite, with locally abundant white to dark red scheelite, without muscovite, fluorite, cassiterite, or beryl. The scheelite typically occurs in both, well developed narrow quartz veins of few cm to dm scale, and in isolated and interconnected quartz pods and veins in, in part, heavily folded and faulted schist. The scheelite is interspersed within the quartz, as granular crystalline masses, ranging in color from pale to yellow and light orange. Locally up to meter size voids are common lined with clear well developed quartz crystals and partially filled with single quartz crystals and clusters. Scheelite in these druses occurs as euhedral and anhedral crystals loose or on quartz. Their color ranges from deep orange to deep red and brown. There is minor apatite within the veins and in the altered wall rock.

We sampled more than 10 mineralized areas, as well as the multiple granite intrusions. Despite often close < 1 km proximity, while likely, no direct structural field relationship between the scheelite occurrences and the granite intrusions could be established.

3. Samples and analysis results

3.1. Samples

About fifteen granite samples were collected from five plutons (Jiantangzhan, Xiaohegou, Dongzi, Mupi, and Wenjiawan) with sample localities shown in Fig. 1, 2A–B. Among these samples eighteen granite samples (Fig. 2C–D) were selected for whole-rock geochemical analysis and a subset of eight for whole-rock Sr, Nd, and Pb isotopic analysis, and five samples were prepared for *in-situ* zircon U–Pb dating.

3.2. Petrography and whole-rock geochemistry

Samples from Jiantangzhan and Mupi are similar, comprised of quartz (~30 %), K-feldspar (~5 %), albite (~50 %), biotite (~15 %), and minor muscovite (Fig. 2E, F). Biotite and muscovite usually form aggregates (Fig. 2E, F). Zircon, apatite, pyrite, and titanite are common accessory minerals. This characterizes Jiantangzhan and Mupi as granodiorite. The samples from Xiaohegou, Dongzi, and Wenjiawan are two-mica granites, comprised of quartz (~30 %), K-feldspar (~25 %), albite (~30 %), biotite (~10 %), and muscovite (~5 %) with gran sizes of 500–1000 μm (Fig. 2E, F). Accessory minerals are zircon, apatite, pyrite, rutile, and fluorite, etc. Note that sample JT-R2A (from Jiantangzhan pluton) may have undergone strong albitization, thus composed of mainly quartz (~10 %), albite (~75 %) and biotite (~15

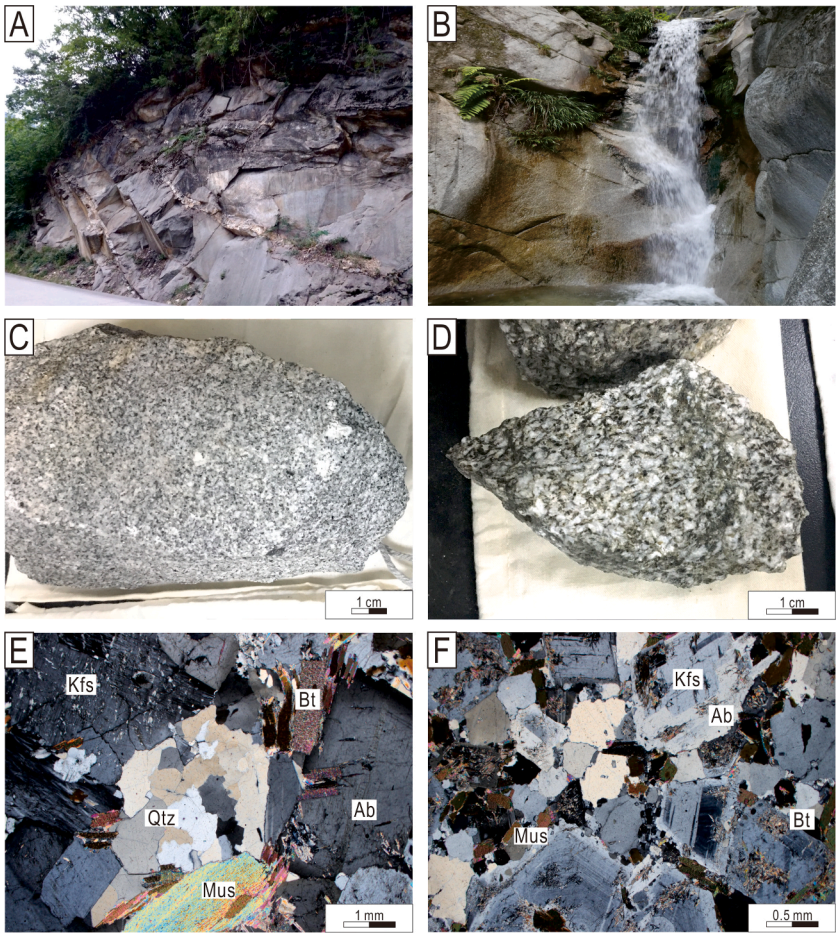

Fig. 2. (A) Photograph of Dongzi two-mica granite outcrops. (B) Photograph of the Wenjiawan granodiorite. (C–D) Representative hand specimens of the sample PW-L1-2–3 and WJ-1, from Dongzi and Wenjiawan plutons respectively. (E–F) Photomicrographs in cross-polarized light of the main rock-forming minerals (muscovite, biotite, albite, and quartz) in the PW-L1-2–3 and WJ-1 samples.

%).

Whole-rock geochemical analyses show that all the granitoids are peraluminous with high A/CNK values [Al_2O_3 / (K_2O + Na_2O + CaO)] from 1.08 to 1.32, except PW-L1-2-3 (0.89; Table 1; Fig. 3). Almost all samples have variable loss-on-ignition (LOI) values (0.45 to 4.68 wt%) and SiO_2 contents of 60.87–73.71 wt% (Table 1). They plot in the medium-K field in a K_2O vs. SiO_2 diagram (Fig. 4A), and granodiorite and granite field in Fig. 4B, with high (Na_2O + K_2O) values of 5.68–8.13 (Table 1) and P_2O_5 varying from 0.07 to 0.13 wt% (Fig. 4C–D). They are depleted in TFe_2O_3 (0.22–2.29 wt%), TiO_2 (0.15–0.89 wt%) and MgO (<1.90 wt%), while enriched in Rb, Ba, Sr, Zr, and Pb, and depleted in Ta, (Fig. 5B). Whole-rock chondrite-normalized REE patterns of all samples are relatively flat with slight light REE enrichment, and negative Eu anomalies (Fig. 5A). Their contents of W, Sn and Be are 0.06–4.07 ppm, 1.04–7.27 ppm and 1.34–12.7 ppm respectively (Table 1).

3.3. U–Pb age of zircon

All U–Pb age data are shown in the Table 2 and Fig. 6. Only a few well-defined zircon crystals from each granitic samples could be found, and used for U–Pb dating. A total of 43 grains from sample XHG-2, WJ-1, PW-L3A, PW-L1-2-3, MP-2 and HYS-2 were analyzed. Their $^{206}Pb/^{238}U$ ages are of 217.0 ± 0.61 Ma (MSWD = 0.92), 223.9 ± 0.88 Ma (MSWD = 0.21), 211.4 ± 0.65 Ma (MSWD = 0.42), 217.1 ± 0.75 Ma (MSWD = 0.65), 217.8 ± 0.60 Ma (MSWD = 3.0) and 229.6 ± 0.60 Ma (MSWD = 1.7) (Table 2; Fig. 6). These ages dates are viewed as the crystallization age of the granitic magma.

3.4. Sr–Nd–Pb isotopes

The calculated Sr–Nd–Pb isotope ratios of representative granite samples are listed in Table 3. All the granite samples show age-corrected initial I_{Sr} ($^{87}Sr/^{86}Sr)_i$ ranging from 0.705888 to 0.714886. These samples also show a range of measured $^{143}Nd/^{144}Nd$ ratios from 0.512048 to 0.512376 with calculated $\varepsilon_{Nd}(t)$ values of −3.49 to −9.51. The granite samples yield two-stage Nd model ages of 1.43–1.77 Ga. The Pb isotope ratios in the granite samples are $^{206}Pb/^{204}Pb$ = 17.9378–18.3996, $^{207}Pb/^{204}Pb$ = 15.5693–15.6836 and $^{208}Pb/^{204}Pb$ = 38.1382–38.7390, respectively (Fig. 7).

4. Discussion

4.1. Comparison of leucogranites in the Xuebaoding and Pingwu areas

Generally, granitoid rocks are classified as I-, S-, and A-types based on chemical and mineralogical criteria (Chappell and White, 1992; Hineab et al., 1978; Whalen et al., 1987). A-type granites are generally enriched in HFSE and REE, with Zr higher than 250 ppm, Zr + Nb + Ce + Y higher than 350 ppm, and high FeOT/MgO ratios (Collins et al., 1982; Eby, 1990,1992; Frost and Frost, 2011). I-type granites always contains hornblende (Chappell and White, 1992; Roberts and Clemens, 1993), and have a low A/CNK value (<1.1; Chappell, 1999; Chappell and White, 1992,1974). S-type granites, derived from metasedimentary rocks typically contain abundant inherited zircons (Collins and Richards, 2008) and Al-rich minerals, such as muscovite, garnet, and cordierite, and are always strongly peraluminous with high A/CNK values (>1.1; Chappell, 1999; Chappell and White, 1992; Clemens, 2003). The Pingwu granites exhibit low FeOT/MgO ratios, low Zr and Zr + Nb + Ce + Y contents, and show a disharmonious trend with respect to the I-type granite field (Fig. 4C). Although some of them can be classified as granodiorite due to its high content of biotite, they contain considerable muscovite, with no hornblende. Combined with their high A/CNK ratios (1.08–1.26; except for the sample PW-L3B; Fig. 3), and the compatible initial Sr values of 0.707–0.715 (except for the 0.706 of sample WJ-1; Fig. 7; Table 3), overall the Pingwu granites should be designated as S-type.

The phenomenon that leucogranitc intrusions exhibit petrological and geochemical heterogeneities is not rare (e.g., Liu et al., 2023a; Tartèse and Boulvais, 2010), which can originate from either primary processes in the source of melts or secondary processes such as fractional crystallization (Wu et al., 2003a; Wu et al., 2003b; Wu et al., 2017). Generally, homologous leucogranites are always closely related temporally and spatially, with continuous variations towards the higher degree of fractionation. For example, plagioclase reflects an evolutionary tend towards the Na end-member during fractionation, and thus, albite granites are generally regarded as the products of extremely fractionated granitic magma (Wu et al., 2003a; Wu et al., 2003b; Li et al., 2007). Similarly, mica exhibits a fractionation sequence from magnesian biotite, magnesian-ferric biotite, zinnwaldite, to lepidolite (Li and Huang, 2013; Li et al., 2015). The highly fractionated granites, in terms of geochemical signatures, are more enriched in SiO_2 and with a higher aluminum saturation index, while depleted in mafic minerals compared with granites of lesser fractionation (Gelman et al., 2014; Lee and Morton, 2015; Wu et al., 2017). Additionally, compared to the common unfractionated or weakly fractionated granites, most highly fractionated granites show a trend with depletion in Cr, Ni, Co, Sr, Ba, and Zr, whereas Li, Rb, Cs, W, Sn, Be, F, Cl, B, and P become enriched during magmatic differentiation (Gelman et al., 2014; Lee and Morton, 2015). Correspondingly, the REE concentrations progressively decrease, as well as the light to heavy REE ratio, and with more pronounced negative Eu anomalies with increasing degree of fractionation (Miller and Mittlefehldt, 1982, 1984; Miller and Miller, 2002; Li and Huang, 2013; Gelman et al., 2014), since Eu is preferentially incorporated into feldspar. (Drake and Weill, 1975).

The Xuebaoding leucogranites which have been classified as typical S-type granites, are primarily exposed and described as the Pukouling and Pankou granites intruding into the Pankou Dome along the core of an anticline (Liu et al., 2010). Spatially, the elevation contrast between the Pingwu and Xuebaoding granites is about 2000 to 3500 m. Temporally, the Pingwu granites are dated ranging from 211.4 ± 0.7 to 229.8 ± 0.6 Ma (Fig. 6; Table 2), which is coeval with the Pankou and Pukouling granites (193.7 ± 1.1 Ma and 200.6 ± 1.2 Ma; Liu et al., 2010; Li et al., 2007). Petrologically, the Pankou and Pukouling plutons have been charactered as highly fractionated albite granites consisting of quartz (35–40 vol%), albite (30–35 vol%), muscovite (30–35 vol%), with minor K-feldspar (0–5 vol%), and minor mafic minerals (Zhang et al., 2021). In contrast, the Pingwu granites analyzed in this study contain higher amounts of K-feldspar and biotite, i.e, a higher mafic content compared to the Xuebaoding granites (Fig. 2E, F).

Geochemically, the Pankou and Pukouling granites show strongly peraluminous signatures (Zhang et al., 2021), with the A/CNK values shown in Fig. 3, and both significantly depleted in Eu (Fig. 5). Besides, the Pankou and Pukouling granites are enriched in Li, Cs, Rb, W, Sn, Be and volatiles (B, P, and F) while concentrations in Ni, Sr, Ba, and Zr are low. In contrast, the Pingwu granites have lower A/CNK values (1.08–1.26, except the sample PW-L1-2-3 is 0.89), and low Li (24.2–125 ppm), Rb (48.2–155 ppm), Cs (2.09–25.9 ppm), W (0.06–1.5 ppm), Sn (1.04–7.27 ppm), and Be (1.64–8.61 ppm) contents, while Sr (178–596 ppm), Ba (482–1080 ppm), and Zr (58–116 ppm) are high (Table 1). ∑REE contents of these granites are relatively high (45.78–90.4 ppm) with no obvious tetrad effect (Fig. 5A). As pointed out by Wu et al. (2017), the Zr/Hf, Nb/Ta, Rb/Sr, and K/Rb ratios are a significant indicator of the degree fractionation of granitic melts. The Pingwu granites display higher Zr/Hf (28.5–34.0), Nb/Ta (4.78–13.8) and K/Rb (3.80–7.32), and lower Rb/Sr (0.05–0.96) ratios (Fig. 8, Table 1) than those reported for Xuebaoding granites (Zr/Hf, Nb/Ta, K/Rb and Rb/Sr of 8.87–19.4, 1.44–4.90, 1.57–2.92 and 2.28–52.8 repectively, Zhang et al., 2021). This combined with the other signatures above, suggests that all granites in the Pingwu and Xuebaoding area are derived from the same magmatic source, yet underwent different degrees of fractionation.

Table 1
Major and trace elements of granites from Pingwu area, Sichuan Province.

Sample	JT-R1	JT-R2A	JT-R2B	JT-R2C	PW-L3A	PW-L3B	XHG-2A	XHG-3B	XHG-4C	XHC2-1-3	PW-L1-2-3	MP-1A	MP-1B	MP-2	MP-3	HYS-1	HYS-2	WJ-1
Pluton	Jiantangzhan							Xiaohegou				Dongzi		Mupi			Wenjianwan	
Wt.%																		
SiO_2	67.00	60.87	65.12	64.51	67.77	66.85	71.41	72.21	73.71	72.03	66.73	68.93	68.67	69.96	69.22	72.25	69.48	68.63
TiO_2	0.40	0.89	0.41	0.37	0.36	0.39	0.19	0.18	0.13	0.15	0.35	0.30	0.22	0.22	0.22	0.22	0.27	0.32
Al_2O_3	16.20	16.55	15.07	15.41	15.78	16.00	15.45	15.32	14.89	14.95	15.46	15.90	16.91	15.68	16.64	15.04	16.01	15.82
TFe_2O_3	1.32	2.29	1.52	0.85	1.05	1.10	0.55	0.32	0.33	0.22	2.72	0.92	0.49	0.83	0.69	0.38	0.98	0.93
FeO	1.53	3.43	2.24	2.16	1.43	1.64	0.88	0.95	0.63	0.89	0.20	1.56	1.28	0.99	1.13	0.92	1.06	1.35
MnO	1.89	3.09	3.45	2.74	1.65	1.84	0.03	0.03	0.02	0.64	0.47	0.04	0.04	0.03	0.04	0.03	0.05	1.88
MgO	0.12	0.17	0.15	0.09	0.11	0.12	0.76	0.68	0.55	0.05	0.10	1.90	1.51	1.52	1.52	0.48	1.42	0.10
CaO	2.67	2.08	2.13	1.87	2.44	2.60	1.29	1.25	1.04	1.42	3.04	2.44	2.37	2.17	2.29	1.74	2.08	2.16
Na_2O	4.41	4.63	3.63	4.06	4.27	4.24	4.09	3.96	4.30	4.28	6.12	5.16	5.87	5.46	5.55	4.20	5.11	5.01
K_2O	2.45	1.58	2.05	2.21	2.87	2.83	3.84	3.66	3.69	3.58	1.58	1.72	1.67	1.64	1.73	3.93	2.22	2.11
P_2O_5	0.10	0.16	0.09	0.08	0.09	0.10	0.13	0.13	0.09	0.10	0.10	0.07	0.07	0.08	0.07	0.07	0.07	0.09
LOI	0.95	4.21	3.74	4.68	1.44	1.45	0.81	0.77	0.70	0.69	3.55	0.69	0.45	0.51	0.50	0.51	0.93	1.42
A/CNK	1.10	1.26	1.24	1.23	1.09	1.08	1.28	1.32	1.24	1.11	0.89	1.27	1.24	1.23	1.27	1.18	1.26	1.09
$Na_2O + K_2O$	6.86	6.21	5.68	6.27	7.14	7.07	7.93	7.62	7.99	7.86	7.70	6.88	7.54	7.10	7.28	8.13	7.33	7.12
Total	99.04	99.95	99.6	99.03	99.26	99.16	99.43	99.46	100.08	99.00	100.42	99.63	99.55	99.09	99.6	99.77	99.68	99.82
ppm																		
La	18.8	13.4	19.1	20.5	17.1	17.3	18.4	16.4	13.0	7.30	10.8	18.6	10.5	10.1	11.3	35.6	14.7	9.40
Ce	38.2	26.1	36.7	41.0	33.3	33.8	34.6	31.6	24.2	13.3	23.3	34.8	19.8	19.4	21.5	52.4	27.8	18.2
Pr	4.30	3.15	4.36	4.56	3.88	3.95	3.39	3.14	2.36	1.68	2.58	3.18	1.94	1.95	2.14	5.27	2.76	2.19
Nd	16.8	13.5	17.2	18.1	15.0	15.1	12.0	10.9	8.09	6.65	10.4	10.7	6.83	6.72	7.58	19.0	10.4	9.00
Sm	3.14	2.97	3.36	3.41	3.06	2.96	2.98	2.64	1.97	1.41	1.95	2.02	1.47	1.47	1.70	3.32	2.31	1.56
Eu	0.77	0.77	0.72	0.75	0.69	0.70	0.58	0.55	0.54	0.42	0.47	0.48	0.39	0.36	0.42	0.70	0.45	0.32
Gd	2.62	2.83	2.89	2.67	2.65	2.76	2.49	2.34	1.71	1.27	1.73	1.59	1.33	1.37	1.55	2.54	2.13	1.42
Tb	0.41	0.45	0.49	0.42	0.43	0.42	0.38	0.38	0.28	0.22	0.26	0.25	0.21	0.24	0.25	0.33	0.37	0.26
Dy	2.31	2.39	2.58	2.22	2.35	2.19	1.95	1.87	1.37	1.07	1.41	1.28	1.20	1.33	1.45	1.46	2.22	1.39
Ho	0.42	0.47	0.49	0.41	0.46	0.41	0.33	0.31	0.24	0.18	0.26	0.25	0.23	0.28	0.29	0.23	0.46	0.27
Er	1.19	1.28	1.38	1.14	1.25	1.14	0.80	0.77	0.61	0.47	0.76	0.69	0.65	0.80	0.84	0.51	1.31	0.78
Tm	0.19	0.20	0.22	0.18	0.21	0.19	0.11	0.11	0.09	0.07	0.12	0.10	0.10	0.12	0.13	0.07	0.19	0.12
Yb	1.09	1.15	1.40	1.09	1.18	1.16	0.73	0.74	0.58	0.46	0.77	0.73	0.67	0.78	0.82	0.44	1.25	0.76
Lu	0.17	0.18	0.22	0.17	0.17	0.17	0.10	0.11	0.08	0.07	0.13	0.11	0.10	0.12	0.12	0.06	0.18	0.12
Hf	3.44	3.36	3.14	3.58	3.37	3.35	2.53	2.54	2.10	1.96	3.29	2.63	2.48	3.01	2.75	4.03	2.89	2.58
Ta	0.60	0.72	0.62	0.62	0.64	0.63	1.92	1.90	1.38	1.77	0.32	0.22	0.27	0.23	0.28	1.46	0.44	0.31
Y	12.7	13.9	15.6	12.6	14.8	14.1	9.49	9.30	7.10	6.13	7.75	6.94	6.56	8.24	8.66	6.55	13.7	8.34
Li	40.9	50.7	59.5	36.0	50.1	57.8	171	141	125	125	24.5	24.1	23.9	24.5	31.8	96.0	39.9	37.4
Be	2.23	1.64	2.85	2.83	2.50	2.91	12.0	10.2	12.7	8.61	1.94	1.34	1.74	1.64	1.84	3.67	1.58	1.65
Sc	6.82	10.7	10.1	8.25	6.89	7.48	4.65	4.07	3.10	3.01	5.10	7.62	5.42	5.48	5.46	2.95	6.55	5.44
V	53.1	64.9	70.2	58.1	49.8	53.7	19.2	17.2	12.5	14.4	52.4	47.1	34.3	34.7	33.7	19.9	42.8	43.2
Cr	35.8	95.3	133	111	34.0	37.5	–	–	–	11.2	44.3	–	–	–	–	–	–	26.3
Ni	30.9	87.5	116	101	27.9	31.8	6.23	5.46	4.38	5.26	71.3	20.1	17.5	18.8	17.5	2.36	11.8	15.4
Cu	9.77	15.9	42.0	33.5	19.6	11.8	5.44	5.39	6.27	7.83	22.2	7.72	1.62	2.18	1.78	18.8	11.8	8.40
Zn	62.5	77.3	75.0	72.1	57.2	64.8	59.4	47.3	34.9	38.7	63.6	59.9	43.7	48.7	44.5	44.2	52.8	53.8
Ga	20.9	20.3	20.9	21.7	20.4	21.5	23.8	22.5	20.1	21.4	18.8	18.8	19.2	19.0	18.8	21.8	18.6	17.5
Rb	87.3	48.2	70.2	82.2	97.7	102	215	201	183	155	50.9	53.7	48.9	50.5	51.2	151	64.5	68.9
Sr	518	178	315	383	507	521	223	218	215	212	454	870	904	875	878	278	675	596
Zr	108	112	96.4	111	110	114	78.4	73.7	67.8	58	105	87.5	79.4	99.5	95.2	132	94.7	79.8
Nb	7.84	8.98	6.92	6.86	7.39	7.95	11.8	10.9	8.37	8.46	4.40	3.27	3.22	3.09	3.29	10.7	5.18	3.70
Mo	0.06	0.09	0.17	0.33	0.06	0.06	<0.05	<0.05	<0.05	0	0.29	<0.05	<0.05	<0.05	<0.05	<0.05	<0.05	0
Cd	<0.05	0.08	<0.05	<0.05	<0.05	0.07	<0.05	<0.05	<0.05	0.05	<0.05	<0.05	<0.05	<0.05	<0.05	<0.05	<0.05	0.06
In	<0.05	<0.05	<0.05	<0.05	<0.05	<0.05	<0.05	<0.05	<0.05	<0.05	<0.05	<0.05	<0.05	<0.05	<0.05	<0.05	<0.05	<0.05
Sn	1.89	1.48	2.11	2.15	1.77	1.91	–	–	–	7.27	1.31	–	–	–	–	–	–	1.04
Sb	0.10	0.52	0.14	0.22	0.14	0.31	–	–	–	0.13	0.23	–	–	–	–	–	–	0.09

(*continued on next page*)

Table 1 (*continued*)

Sample	JT-R1	JT-R2A	JT-R2B	JT-R2C	PW-L3A	PW-L3B	XHG-2A	XHG-3B	XHG-4C	XHC2-1-3	PW-L1-2-3	MP-1A	MP-1B	MP-2	MP-3	HYS-1	HYS-2	WJ-1
Pluton	Jiantangzhan							Xiaohegou				Dongzi		Mupi			Wenjianwan	
Cs	3.23	2.09	3.43	4.11	4.4	4.82	20.4	18.9	16.3	25.9	2.72	6.47	3.05	5.28	6.80	7.30	2.29	2.56
Ba	685	452	482	579	755	721	569	547	530	572	571	698	740	767	781	710	1127	1072
W	0.34	4.07	0.78	2.49	0.22	0.18	1.09	0.99	0.82	0.63	1.50	0.33	0.15	0.12	0.14	0.34	0.17	0.06
Tl	0.38	0.21	0.27	0.36	0.39	0.40	1.07	1.04	0.93	0.79	0.24	0.26	0.24	0.23	0.24	0.63	0.34	0.33
Pb	22.2	6.43	21.1	23.0	25.3	21.9	37.8	38.7	35.8	51.7	23.5	12.7	15.8	14.6	16.0	27.3	17.9	17.0
Bi	0.14	<0.05	0.55	0.35	0.31	0.12	1.34	1.44	1.44	1.51	0.14	<0.05	<0.05	<0.05	0.05	0.37	<0.05	<0.05
Th	6.58	3.82	7.33	8.14	6.11	5.84	6.20	5.42	4.12	3.22	3.33	4.56	2.73	2.64	2.75	14.5	4.12	3.29
U	0.85	1.13	1.71	2.07	1.23	1.46	2.15	2.07	1.77	1.04	0.80	0.44	0.40	0.49	0.82	1.82	0.78	0.70
Co	7.81	21.0	16.1	12.6	6.85	7.67	2.94	2.68	2.08	2.35	9.70	6.16	4.92	5.03	4.97	2.41	4.78	5.07
Rb/Sr	0.17	0.27	0.22	0.21	0.19	0.20	0.96	0.92	0.85	0.73	0.11	0.06	0.05	0.06	0.06	0.54	0.10	0.12
K/Rb	5.97	6.97	6.21	5.72	6.25	5.90	3.80	3.87	4.29	4.91	6.60	6.81	7.27	6.91	7.19	5.54	7.32	6.52
Zr/Hf	31.4	33.3	30.7	31.0	32.6	34.0	30.99	29.02	32.29	29.6	31.9	33.3	32.0	33.1	34.6	32.8	32.8	30.9
Nb/Ta	13.1	12.5	11.2	11.1	11.5	12.6	6.15	5.74	6.07	4.78	13.8	14.9	11.9	13.4	11.8	7.33	11.8	11.9
∑REY	103	82.7	107	109	96.5	96.4	88.3	81.2	62.2	40.7	62.7	81.7	52.0	53.3	58.8	128	80.2	54.1
Estimated T (°C)	795	801	791	802	797	799	777	773	765	747	779	777	769	789	786	815	786	770

"-" no determination.

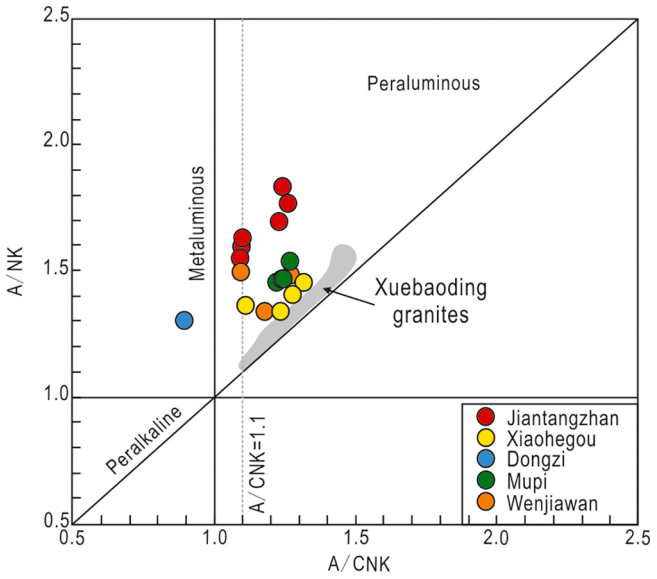

Fig. 3. Ratios of A/NK (Al_2O_3/ [Na_2O + K_2O]) vs. A/CNK (Al_2O_3/ [CaO + Na_2O + K_2O]) (based on Maniar and Piccoli, 1989) for the Pingwu and Xuebaoding granites. Data of Pankou and Pukouling granites (grey) taken from Zhang et al., 2021.

4.2. Global comparison of W–Sn–Be mineralization with that of the Xuebaoding area

Although are all closely associated with evolved granites derived from the anatexis of metasedimentary rocks, W, tin (Sn and Be deposits are generally separated both temporally and spatially. This is demonstrated for the range of globally significant W an Sn belts, where only 3 of 77 Sn deposits in China (Chang et al., 2019), and 6 of 69 in the Bolivian Sn belt (Clark et al., 1990; Mlynarczyk and Williams-Jones, 2005; Arce-Burgoa and Goldfarb, 2009) contain appreciable W in addition to Sn concentrations, let alone Be. Generally, the nature of the magmatic source, the melting temperature, and subsequent magmatic-hydrothermal evolution, together contribute to the W–Sn–Be metallogenic behaviors. Worldwide, the bulk W, Sn, and Be resources are hosted by magmatic-hydrothermal ore deposits associated with highly fractionated S-type granitic intrusions (Lehmann, 1990; Brown and Pitfield, 2014; Liu et al., 2023a), derived from the partial melting of metapelitic rocks enriched in incompatible elements e.g., W, Sn, and Be (Ishihara, 1977; Romer and Kroner, 2016; Gardiner et al., 2017). Such fertilized sources, however, may face the challenge of partial melting temperature, which enables the releasing of rare-metal elements involved. By comparison, the incorporation of Sn into magma requires a temperature partial melting via biotite-dehydration (ca. 800 ℃), which is 50 ℃ higher than the muscovite-dehydration melting corresponding to the release of W (Zhao et al., 2022). And it is noteworthy that among the protolith minerals, the mineral melt partition coefficients of Be is also highest for muscovite and cordierite (Simons et al., 2017). This implies that even the simultaneously presence of high concentrations of, e.g., W, Sn, and Be by the fertilized magmatic source, a suitably high temperature is still required for the simultaneous release of multiple elements. Miller et al. (2003) optimized the zircon saturation temperature (T_{Zr}) calculation, so that one can estimate from bulk-rock Zr concentration Zr_{melt} (in ppm) a minimum temperature if the magma was undersaturated, or a maximum temperature if it was saturated:

$$T_{Zr} = 12900/[2.95 + 0.85M + ln(496000/Zr_{melt})]$$

where M is the cation fraction of the compositional factor that accounts for the dependence of zircon solubility on SiO_2 and peraluminosity of the melt, with M given by

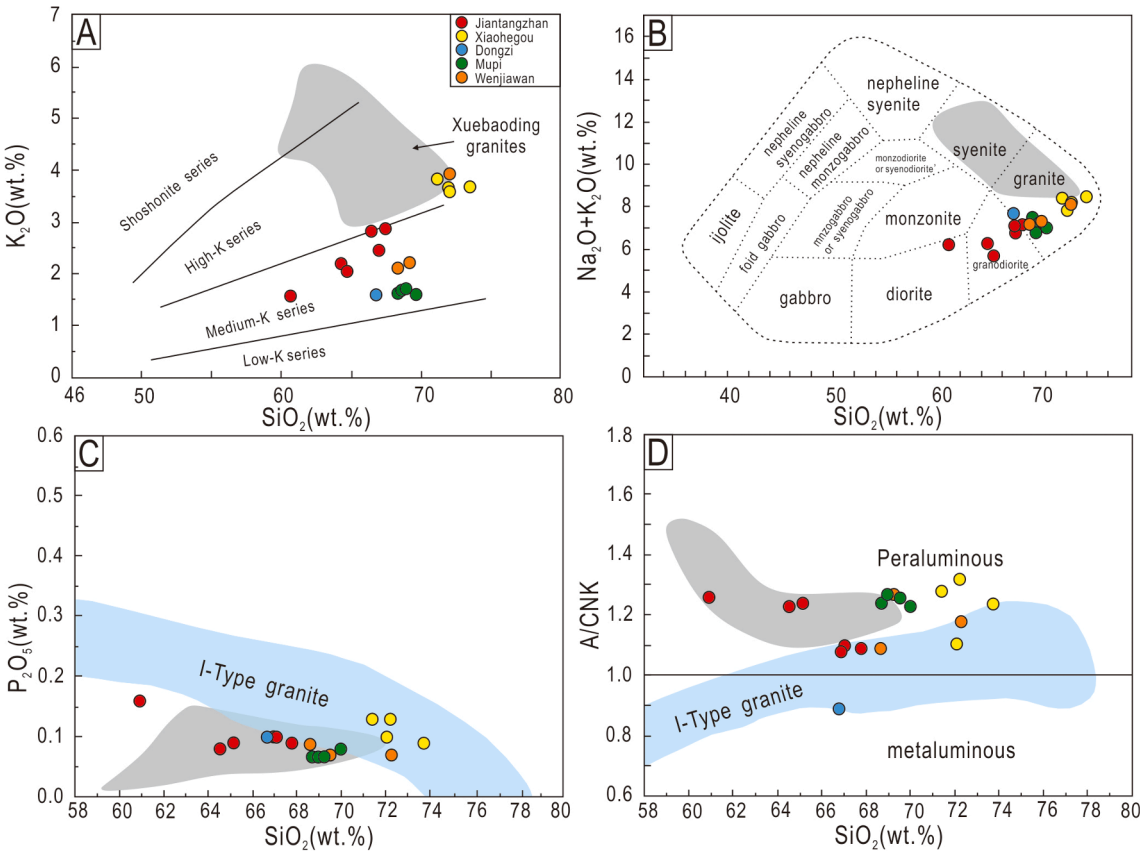

Fig. 4. Plots of (A) K_2O vs. SiO_2 (Gill, 1981), (B) ($Na_2O + K_2O$) vs. SiO_2 (Middlemost, 1994), (C) P_2O_5 vs. SiO_2, and (D) A/CNK vs. SiO_2 for the Pingwu and Xuebaoding granites. The trends in (C) and (D) for I-type granite are from Chappell (1999). Data of Pankou and Pukouling granites (grey) taken from Zhang et al., 2021.

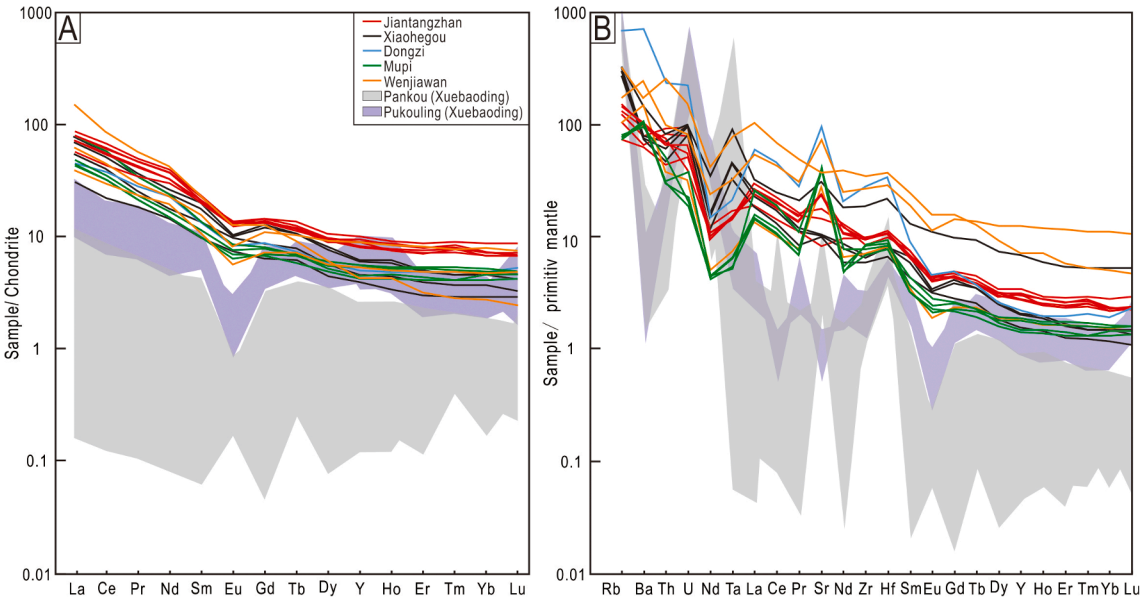

Fig. 5. (A) Chondrite-normalized rare earth element and (B) primitive-mantle-normalized trace element patterns for the Pingwu and Xuebaoding granites. Data of Pankou (grey) and Pukouling granites (purple) taken from Zhang et al., 2021. (For interpretation of the references to color in this figure legend, the reader is referred to the web version of this article.)

$$M = [(Na + K + 2 \times Ca)/(Al \times Si)]$$

with temperature T_{Zr} in Kelvin. This empirical equation can then be used to estimate the melting temperatures of the granites from Pingwu, ranging from ca. 747 to 815 ℃ (Table 1). Considering the moderate Zr content in these granites (Table 2), these temperatures are generally lower than the typical values where Sn tends to get released into the melts (at > 800℃), while higher than what is necessary for the release of

Table 2
LA-ICPMS zircon U–Pb data of granites from the Pingwu area.

Sample	Pluton	Element (ppm)	Th/U			Isotope ratio										Age (Ma)			
		Pb	Th	U		$^{207}Pb/^{206}Pb$	±1σ	$^{207}Pb/^{235}U$	±1σ	$^{206}Pb/^{238}U$	±1σ	$^{208}Pb/^{232}Th$	±1σ	$^{207}Pb/^{235}U$	±1σ	$^{206}Pb/^{238}U$	±1σ	$^{207}Pb/^{206}Pb$	±1σ
PW-L3A-3	Jiantangzhan	20.9	263	535	0.5	0.0509	0.0015	0.2344	0.0056	0.0333	0.0003	0.0109	0.0002	213.8	4.6	211.4	1.9	235.3	66.7
PW-L3A-4		17.5	195	448	0.4	0.0505	0.0010	0.2325	0.0045	0.0334	0.0003	0.0105	0.0002	212.3	3.8	211.9	1.6	216.7	46.3
PW-L3A-7		19.9	249	504	0.5	0.0507	0.0010	0.2328	0.0044	0.0333	0.0002	0.0107	0.0001	212.5	3.6	211.0	1.4	233.4	41.7
PW-L3A-8		21.8	255	556	0.5	0.0505	0.0010	0.2323	0.0044	0.0333	0.0002	0.0108	0.0002	212.1	3.7	211.2	1.5	216.7	48.1
PW-L3A-11		19.8	202	483	0.4	0.0506	0.0016	0.2318	0.0066	0.0335	0.0003	0.0105	0.0002	211.7	5.4	212.2	1.7	233.4	74.1
PW-L3A-12		19.3	234	467	0.5	0.0505	0.0012	0.2321	0.0054	0.0333	0.0002	0.0105	0.0002	212.0	4.5	210.9	1.5	220.4	53.7
XHG-2-1	Xiaohegou	245	282	6876	0.0	0.0510	0.0006	0.2407	0.0033	0.0341	0.0003	0.0122	0.0004	219.0	2.7	216.4	2.0	239.0	25.9
XHG-2-2		252	312	6806	0.1	0.0502	0.0006	0.2383	0.0029	0.0343	0.0002	0.0126	0.0008	217.0	2.4	217.5	1.4	205.6	27.8
XHG-3-5		218	308	5824	0.1	0.0488	0.0006	0.2354	0.0058	0.0345	0.0003	0.0117	0.0014	214.7	4.7	218.4	2.0	139.0	41.7
XHG-2-7		254	280	7196	0.0	0.0497	0.0005	0.2349	0.0025	0.0341	0.0002	0.0116	0.0002	214.3	2.1	216.5	1.5	189.0	22.2
XHG-2-11		318	536	7913	0.1	0.0497	0.0009	0.2402	0.0055	0.0343	0.0004	0.0119	0.0010	218.6	4.5	217.4	2.5	189.0	40.7
XHG-2-12		189	200	5323	0.0	0.0498	0.0005	0.2357	0.0030	0.0342	0.0003	0.0109	0.0002	214.9	2.5	216.6	1.7	183.4	21.3
XHG-2-15		492	776	13,011	0.1	0.0494	0.0013	0.2352	0.0057	0.0341	0.0002	0.0158	0.0015	214.5	4.7	216.2	1.4	164.9	65.7
XHG-2-16		387	305	8432	0.0	0.0489	0.0015	0.2368	0.0082	0.0344	0.0003	0.0111	0.0037	215.8	6.7	218.3	1.8	142.7	69.4
PW-L3-01	Dongzi	58.1	791	1364	0.6	0.0507	0.0009	0.2420	0.0046	0.0346	0.0003	0.0109	0.0002	220.1	3.7	219.5	2.2	227.8	42.6
PW-L3-02		46.6	498	1164	0.4	0.0504	0.0011	0.2408	0.0056	0.0346	0.0004	0.0109	0.0002	219.0	4.6	219.1	2.3	213.0	51.8
PW-L3-03		61.1	690	1462	0.5	0.0496	0.0010	0.2364	0.0045	0.0347	0.0003	0.0111	0.0002	215.4	3.7	219.6	2.2	176.0	46.3
PW-L3-14		43.0	478	1049	0.5	0.0508	0.0011	0.2407	0.0054	0.0344	0.0003	0.0111	0.0002	219.0	4.4	218.1	2.1	231.6	45.4
PW-L3-16		36.7	386	904	0.4	0.0502	0.0012	0.2382	0.0053	0.0348	0.0004	0.0110	0.0002	216.9	4.3	220.3	2.4	211.2	53.7
PW-L3-19		47.9	525	1182	0.4	0.0521	0.0012	0.2454	0.0055	0.0342	0.0003	0.0108	0.0002	222.8	4.5	216.5	2.2	300.1	50.0
PW-L3-11		52.5	740	1270	0.6	0.0514	0.0011	0.2374	0.0049	0.0335	0.0003	0.0107	0.0002	216.3	4.0	212.2	2.0	257.5	48.1
PW-L3-09		47.8	561	1205	0.5	0.0513	0.0010	0.2370	0.0050	0.0335	0.0003	0.0106	0.0002	216.0	4.1	212.2	2.2	253.8	46.3
MP-2-04	Mupi	84.3	683	2084	0.3	0.0517	0.0011	0.2466	0.0057	0.0345	0.0005	0.0113	0.0003	223.8	4.6	218.7	3.2	333.4	41.7
MP-2-05		81.7	712	2081	0.3	0.0507	0.0011	0.2400	0.0062	0.0341	0.0005	0.0103	0.0003	218.5	5.0	215.9	3.3	227.8	50.0
MP-2-09		61.3	549	1434	0.4	0.0527	0.0013	0.2617	0.0069	0.0357	0.0006	0.0132	0.0003	236.0	5.5	226.4	3.6	316.7	55.6
MP-2-11		84.1	641	2028	0.3	0.0523	0.0011	0.2582	0.0066	0.0355	0.0006	0.0136	0.0004	233.2	5.3	225.0	3.9	298.2	48.1
MP-2-13		69.7	567	1778	0.3	0.0529	0.0011	0.2454	0.0057	0.0334	0.0005	0.0113	0.0002	222.9	4.7	212.0	3.2	327.8	46.3
MP-2-14		107	1167	2616	0.4	0.0507	0.0010	0.2371	0.0050	0.0337	0.0005	0.0106	0.0002	216.1	4.1	213.7	2.8	227.8	75.0
HYS-2-4	Wenjiawan	44.4	772	950	0.8	0.0498	0.0007	0.2509	0.0039	0.0363	0.0003	0.0106	0.0001	227.3	3.1	229.7	1.7	187.1	31.5
HYS-2-5		27.1	490	579	0.8	0.0512	0.0009	0.2560	0.0044	0.0362	0.0003	0.0114	0.0001	231.4	3.5	229.1	1.7	250.1	38.9
HYS-2-7		63.7	1208	1353	0.9	0.0515	0.0008	0.2578	0.0036	0.0362	0.0003	0.0115	0.0001	232.9	2.9	229.2	1.7	264.9	33.3
HYS-2-10		40.1	835	837	1.0	0.0507	0.0010	0.2570	0.0042	0.0366	0.0003	0.0115	0.0001	232.2	3.4	231.5	2.1	227.8	75.0
HYS-2-11		86.3	1721	1546	1.1	0.0503	0.0023	0.2525	0.0116	0.0360	0.0003	0.0114	0.0002	228.6	9.4	228.0	2.2	209.3	103.7
HYS-2-13		75.8	1183	1633	0.7	0.0500	0.0011	0.2512	0.0059	0.0363	0.0003	0.0101	0.0002	227.5	4.8	230.0	2.1	194.5	50.0
HYS-2-19		38.4	560	847	0.7	0.0514	0.0010	0.2588	0.0041	0.0364	0.0003	0.0121	0.0001	233.7	3.3	230.7	1.8	261.2	46.3
HYS-2-21		55.6	511	1431	0.4	0.0510	0.0010	0.2533	0.0040	0.0359	0.0003	0.0086	0.0002	229.3	3.2	227.2	2.0	239.0	48.1
HYS-2-22		32.7	640	671	1.0	0.0508	0.0012	0.2544	0.0043	0.0363	0.0003	0.0120	0.0001	230.2	3.5	230.1	1.7	231.6	55.5
HYS-2-26		20.4	458	412	1.1	0.0512	0.0011	0.2567	0.0057	0.0362	0.0003	0.0117	0.0002	232.0	4.6	229.5	2.1	250.1	51.8
WJ-1-2		32.1	308	810	0.4	0.0494	0.0011	0.2407	0.0052	0.0355	0.0003	0.0112	0.0002	219.0	4.2	224.9	2.1	168.6	50.0
WJ-1-3		48.0	561	1160	0.5	0.0507	0.0010	0.2475	0.0052	0.0353	0.0003	0.0108	0.0002	224.5	4.2	223.8	1.9	227.8	41.7
WJ-1-4		41.2	422	1020	0.4	0.0503	0.0010	0.2461	0.0051	0.0353	0.0003	0.0121	0.0002	223.4	4.2	223.9	2.1	209.3	44.4
WJ-1-12		25.3	200	638	0.3	0.0502	0.0012	0.2444	0.0061	0.0354	0.0003	0.0117	0.0003	222.0	5.0	224.5	2.1	205.6	57.4
WJ-1-13		39.1	449	930	0.5	0.0509	0.0008	0.2480	0.0039	0.0352	0.0003	0.0114	0.0001	224.9	3.2	223.1	1.7	235.3	61.1

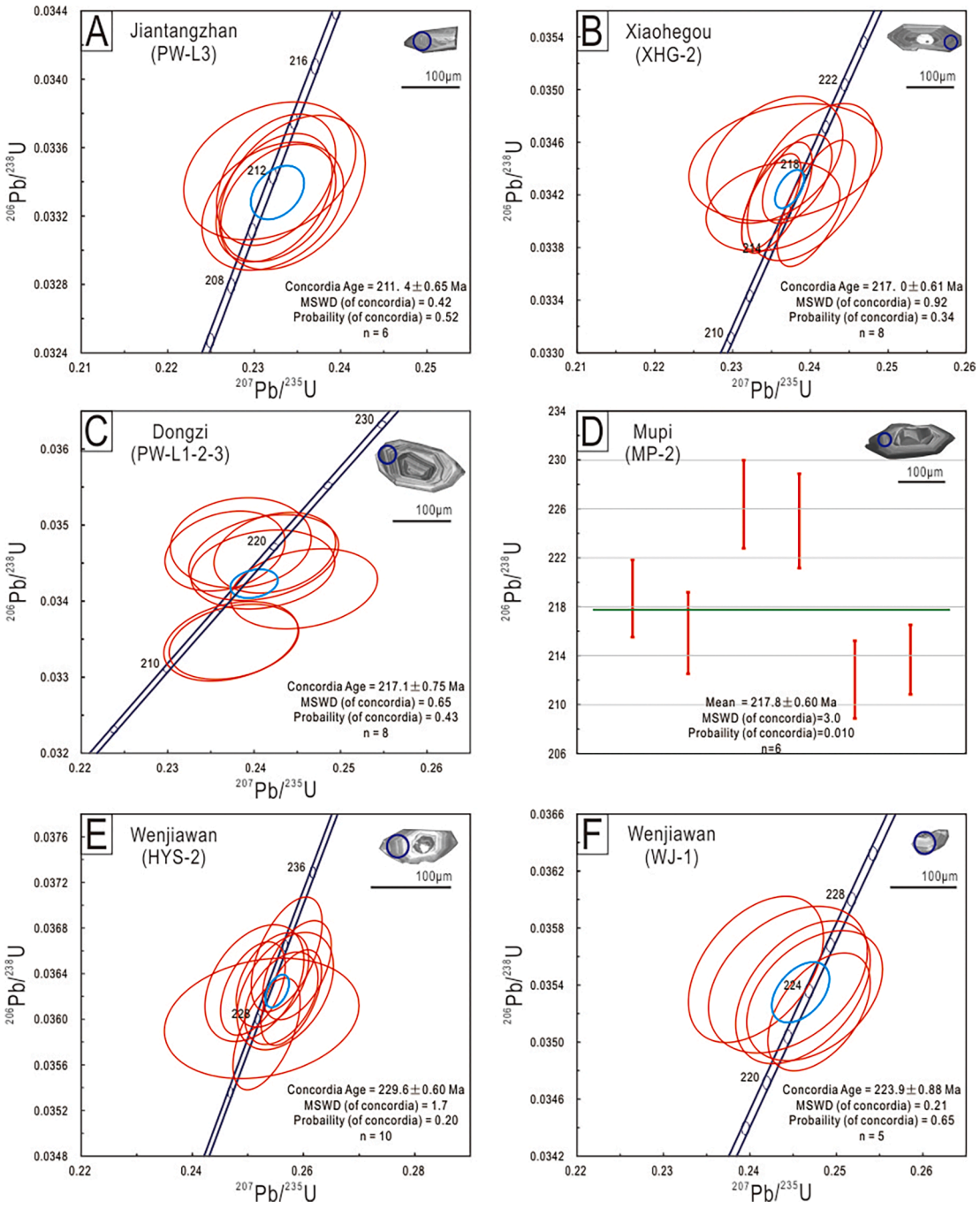

Fig. 6. LA-ICP-MS Zircon U–Pb concordia ages of the Pingwu granites.

Table 3
Sr-Nd-Pb isotope composition of granites from the Pingwu area, Sichuan Province, SW China.

Sample	Pluton	$^{206}Pb/^{204}Pb$	$^{207}Pb/^{204}Pb$	$^{208}Pb/^{204}Pb$	$^{87}Rb/^{86}Sr$	$^{87}Sr/^{86}Sr$	$^{87}Sr/^{86}Sr_{(i)}$	$^{147}Sm/^{144}Nd$	$^{143}Nd/^{144}Nd$	$\varepsilon Nd_{(i)}$	T_{DM2}(Ga)
JT-R1	Jiantangzhan	18.2957	15.5780	38.5234	0.8072	0.710015	0.707719	0.1330	0.512376	−3.49	1.46
JT-R2A		18.1039	15.5890	38.3671	0.6643	0.711482	0.709593	0.1181	0.512048	−9.51	1.75
JT-R2B		18.0846	15.5769	38.4353	0.6398	0.711616	0.709796	0.1139	0.512061	−9.15	1.66
PW-L3A		18.0825	15.5889	38.3872	0.5744	0.708356	0.706722	0.1233	0.512099	−8.64	1.77
PW-L3B		18.0802	15.5890	38.4121	0.5836	0.708308	0.706648	0.1185	0.512104	−8.42	1.67
XHG2-1-3	Xiaohegou	18.3996	15.6836	38.7390	2.1795	0.721065	0.714866	0.1036	0.512069	−8.73	1.50
PW-L1-2-3	Dongzi	18.1708	15.6370	38.6148	0.3342	0.708928	0.707977	0.1133	0.512209	−6.24	1.43
WJ-	Wenjiawan	17.9378	15.5693	38.1382	0.3446	0.706868	0.705888	0.1048	0.512114	−7.88	1.45

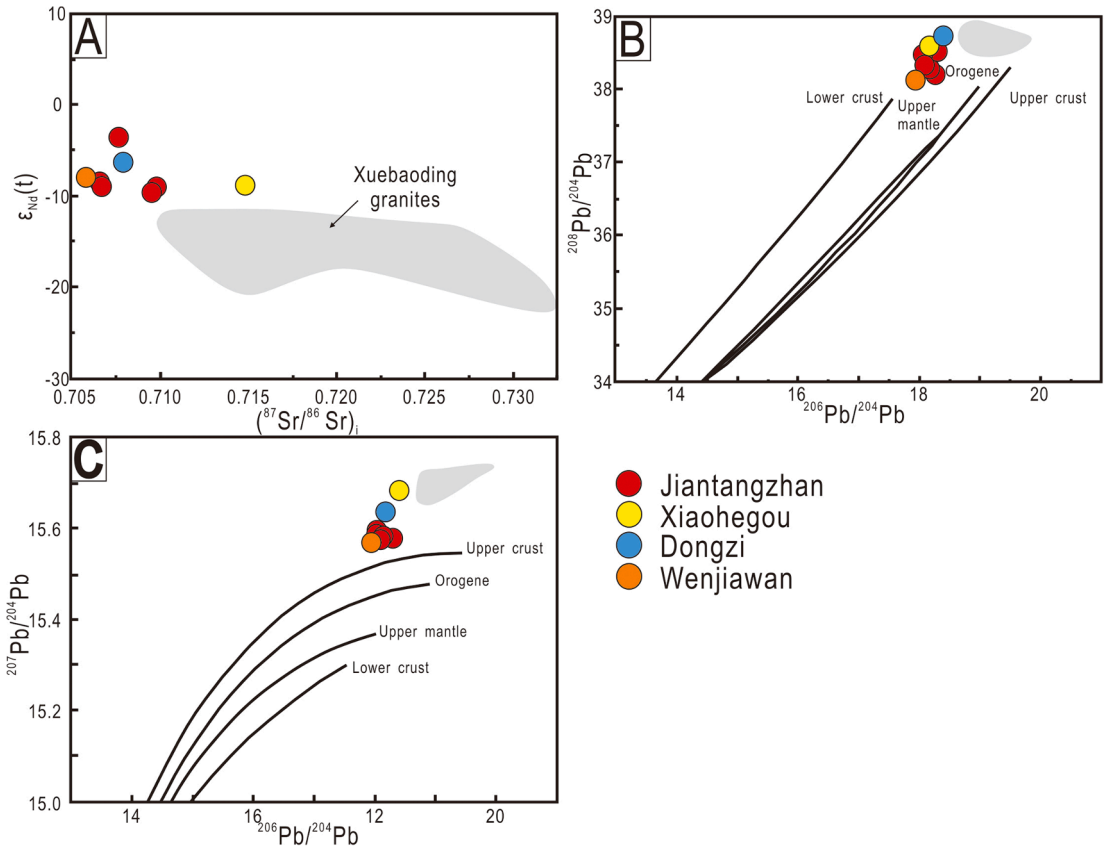

Fig. 7. (A) Plots of (A) εNd(t) vs. $(^{87}Sr/^{86}Sr)_i$, (B) $^{208}Pb/^{204}Pb$ vs. $^{206}Pb/^{204}Pb$, and (C) $^{207}Pb/^{204}Pb$ vs. $^{206}Pb/^{204}Pb$ for the Pingwu and Xuebaoding area granites, data of Pankou and Pukouling granites (grey) taken from Zhang et al., 2021.

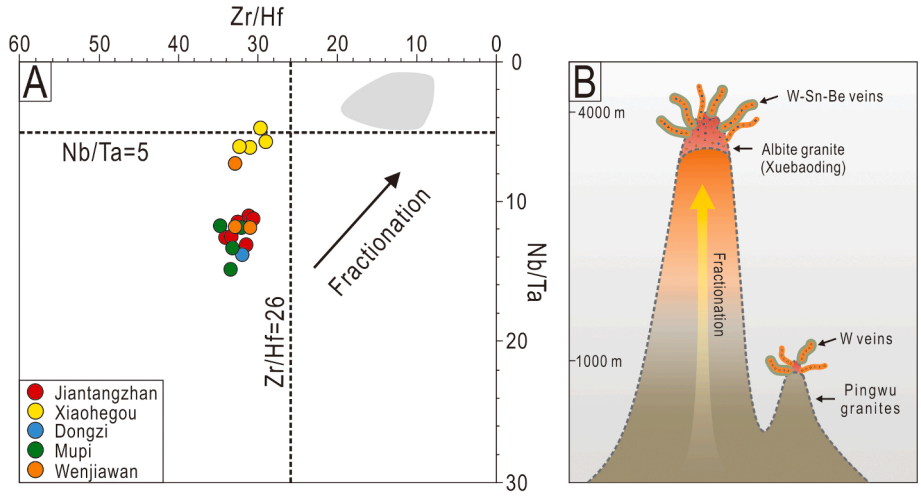

Fig. 8. (A) Nb/Ta vs. Zr/Hf ratios for the granites from the Pingwu and Xuebaoding area showing the fractionation degree (of which the trend taken from Wu et al., 2017). Data of Pankou and Pukouling granites (grey) taken from Zhang et al., 2021. (B) Schematic diagram of Xuebaoding and Pingwu area.

W (ca. 750℃) (Zhao et al., 2022). This may explain the significantly lower content of W, Sn, and Be in the Pingwu system (0.18–4.07, 1.04–7.27, and 1.34–8.61 ppm, respectively), compared to the values in Xuebaoding granites (2.07–54.1, 41.3–200, and 6.73–1681 ppm, respectively; Zhang et al., 2021), even though both the Xuebaoding and Pingwu granites are derived from the same magmatic source.

Yet even in such low concentrations, the Pingwu areas still exhibit large-scale and exclusive tungsten mineralization. Rare metals, as incompatible elements, require a high concentration in the magmatic-hydrothermal systems to reach saturation. Fractionation have been shown to further amplify the W, Sn, and Be concentrations in magmas (Wu et al., 2017). These concentrations are important for the W–Sn–Be mineralization potential because elevated W, Sn and Be concentrations in the exsolved magmatic-hydrothermal fluids are indicators of the type and extent of mineralization (Audétat, 2019). The rare-metal element concentrations under closed and stable fractionating condition continue to rise until crystallization sets in once saturation conditions are reached (Liu et al., 2023b; Zhao et al., 2022). Fig. 8 shows the obviously increase in the degree of fractionation from Pingwu granites to albite granite which could readily explain the W–Sn–Be mineralization in the

Xuebaoding area. In contrast the fractionation seems less developed for the occurrences of the Pingwu area known for only scheelite, with minor apatite, and the absence of cassiterite and beryl.

Although fractionation is certainly one of the critical steps promoting mineralization and enrichment, in unfractionated magmas, the mobility signatures of rare metals are particularly significant. Generally, Be forms chloride and fluoride complexes in magmatic-hydrothermal systems, of which the saturation requires extreme fractionation and low temperatures (London, 2008,2015). The solubility of SnO_2, which always forms as series of stannous chloride-bearing species in alkali chloride-bearing acid solutions, is limited by decreasing fluid acidity and oxidized conditions, with little influence by temperature (Taylor and Wall, 1993; Liu et al., 2023a). In contrast, tungsten forms mainly as H_2WO_4, HWO_4^-, WO_4^{2-}, $NaWO_4^-$, Na_2WO_4 in high temperature hydrothermal systems, and its concentration increases strongly with increasing temperature, NaCl content, and pH value concomitantly (Wood and Samson, 2000; Wang et al., 2020). Therefore, premature destruction of the enclosed environment is likely to be detrimental to attain the saturation of Sn and Be but minimally affects W, in magmatic-hydrothermal systems. This appears to be the case for the W mineralization in the Pingwu areas where the magmas exhibit a relatively lower degree of fractionation and low W contents, yet the unique mobility of W can still enable its continuously enrichment and mineralization.

5. Conclusions and further implications

Our model shows that the temperature and degree of partial melting of an appropriate protolith, the fractionation of melts and the migration behavior of W, Sn, and Be in magmatic-hydrothermal systems determines whether the resulting granites will trend towards mono- or polymetallic mineral deposits. A fertilized magmatic source and its incongruent partial melting might play an important role in the formation of such deposits. The fractionation of magma is also a key factor leading to the continuous enrichment of rare metals. Additionally, in a melt of lower degree of fractionation, of which the ore-element concentration has not yet attained the saturation crystallization required, the unique migration signature of certain elements (e.g., W) may overcome these constraints and lead to mineralization. Such model may also apply to the formation of deposits of other metals (e.g., Ta and Li deposits), which are also genetically related to highly evolved S-type granites (Romer and Kroner, 2016).

CRediT authorship contribution statement

Xinxiang Zhu: Writing – original draft. **Markus B. Raschke:** Writing – review & editing. **Yan Liu:** Funding acquisition.

Declaration of competing interest

The authors declare that they have no known competing financial interests or personal relationships that could have appeared to influence the work reported in this paper.

Data availability

Data will be made available on request.

Acknowledgements

This research was funded by the Second Tibetan Plateau Scientific Expedition and Research (Grant 2021QZKK0304) and China Geological Survey Program, Ministry of Natural Resources (Grant DD 20221649). MBR would like to thank Ping Wang, Zhe Li, and members of the Huya, Kuoda, Shuijing, and Pingwu mining community for invaluable support with the geologic field work.

Appendix A. Supplementary data

Supplementary data to this article can be found online at https://doi.org/10.1016/j.oregeorev.2024.105933.

References

Arce-Burgoa, O.R., Goldfarb, R.J., 2009. Metallogeny of Bolivia. Soc. Econ. Geol. Newslett. 79 (1), 8–12.
Audétat, A., 2019. The metal content of magmatic-hydrothermal fluids and its relationship to mineralization potential. Econ. Geol. 114, 1033–1056.
Bettencourt, J.S., Leute Jr., W.B., Goraieb, C.L., Sparrenberger, I., Bello, R.M.S., Payolla, B.L., 2005. Sn-polymetallic greisen-type deposits associated with late-stage rapakivi granites, Brazil: fluid inclusion and stable isotopes characteristics. Lithos 80, 363–386.
Blevin, P.L., Chappell, B.W., 1992. The role of magma sources, oxidation states and fractionation in determining the granite metallogeny of eastern Australia. Earth Environ. Sci. Trans. R. Soc. Edinb. 83, 305–316.
Blevin, P.L., Chappell, B.W., 1995. Chemistry, origin, and evolution of mineralized granites in the Lachlan fold belt, Australia: The metallogeny of I- and S-type granites. Econ. Geol. 90, 1604–1619.
Brown, T., Pitfield, P., 2014. Tungsten. In: Gunn, G. (Ed.), Critical Metals Handbook: Oxford. John Wiley and Sons, UK, pp. 385–409.
Cao, Z.M., Zheng, J.B., Li, Y.G., Ren, J.G., Xu, S.J., Wang, R.C., Shoji, T., Kaned, H., Kabayashi, S., 2002. Geologic and geochemical features of the volatile-rich ore fluid and its tracing and dating in the Xuebaoding Beryl-Scheelite Vein Deposit, China. Sci. China 45, 719–729.
Cao, Z.M., Zheng, J.P., An, W., Li, Y.G., 2004. Geochemistry of Xuebaoding alkali granite and its ore-controlling effect. J. Ocean Univ. Qingdao 34, 874–880 in Chinese with English abstract.
Černý, P., Ercit, T.S., 2005. The classification of granitic pegmatites revisited. Can. Mineral. 43, 2005–2026.
Chakhmouradian, A.R., Smith, M.P., Kynicky, J., 2015. From "strategic" tungsten to "green" neodymium: A century of critical metals at a glance. Ore Geol. Rev. 64, 455–458.
Chang, Z.S., Shu, Q.H., Meinert, L.D., 2019. Skarn deposits of China, in Chang, Z.S., and Goldfarb, R.J., eds., Mineral Deposits of China. Society of Economic Geologists Special Publication 22, 189–234.
Chappell, B.W., 1999. Aluminium Saturation in I- and S-Type Granites and the Characterization of Fractionated Haplogranites. Lithos 46 (3), 535–551.
Chappell, B.W., White, A.J.R., 1974. Two contrasting granite types. Pac. Geol. 8, 173–174.
Chappell, B.W., White, A.J.R., 1992. I- and S-type granites in the Lachlan Fold Belt. Transactions of the Royal Society of Edinburgh. Earth Sci. 83, 1–26.
Clark, A.H., et al., 1990. Geologic and geochronologic constraints on the metallogenic evolution of the Andes of southeastern Peru. Econ. Geol. 85, 1520–1583.
Clemens, J.D., 2003. S-type granitic magmas-petrogenetic issues, models and evidence. Earth Sci. Rev. 61 (1/2), 1–18.
Collins, W.J., Beams, S.D., White, A.J.R., Chappell, B.W., 1982. Nature and Origin of A-Type Granites with Zoneicular Reference to Southeastern Australia. Contrib. Miner. Petrol. 80 (2), 189–200.
Collins, W.J., Richards, S.W., 2008. Geodynamic significance of S-type granites in circum-Pacific orogens. Geology 36 (7), 559–562.
Drake, M.J., Weill, D.F., 1975. Partition of Sr, Ba, Ca, Y, Eu2+, Eu3+, and other REE between plagioclase feldspar and magmatic liquid: an experimental study. Geochim. Cosmochim. Acta 39 (5), 689–712.
Eby, G.N., 1990. The a-Type Granitoids - a Review of Their Occurrence and Chemical Characteristics and Speculations on Their Petrogenesis. Lithos 26 (1–2), 115–134.
Eby, G.N., 1992. Chemical Subdivision of the a-Type Granitoids - Petrogenetic and Tectonic Implications. Geology 20 (7), 641–644.
Esmaeily, D., Nedelecb, A., Valizadeh, M.V., Moorec, F., Cottend, J., 2005. Petrology of the Jurassic Shah-Kuh granite (eastern Iran), with reference to tin mineralization. J. Asian Earth Sci. 25, 961–980.
Frost, C.D., Frost, B.R., 2011. On Ferroan (A-type) Granitoids: their Compositional Variability and Modes of Origin. J. Petrol. 52 (1), 39–53.
Gardiner, N.J., Hawkesworth, C.J., Robb, L.J., Whitehouse, M.J., Roberts, N.M.W., Kirkland, C.L., Evans, N.J., 2017. Contrasting granite metallogeny through the zircon record: A case study from Myanmar. Sci. Rep. 7, 748.
Gelman, S.E., Deering, C.D., Bachmann, O., Huber, C., Gutiérrez, F.J., 2014. Identifying the crystal graveyards remaining after large silicic eruptions. Earth Planet. Sci. Lett. 403, 299–306.
Gill, T.B., 1981. Orogenic Andesite and Plate Tectonics: Berlin, Springer-Verlag, 390.
Hineab, R., Williamscd, I.S., Chappelle, B.W., White, A.J.R., 1978. Contrasts between I- and S-type granitoids of the Kosciusko Batholith. J. Geol. Soc. Aust. 25 (3–4), 219–234.
Ishihara, S., 1977. The magnetite-series and ilmenite-series granitic rocks. Mining Geol. 27, 293–305.
Kirby, E., Ouimet, W., 2011. Tectonic geomorphology along the eastern margin of tibet: insights into the pattern and processes of active deformation adjacent to the sichuan basin. Geol. Soc. Lond. Spec. Publ. 353 (1), 358–361.
Lee, C.T.A., Morton, D.M., 2015. High silica granites: Terminal porosity and crystal settling in shallow magma chambers. Earth Planet. Sci. Lett. 409, 23–31.
Lehmann, B., 1990. Metallogeny of Tin: Berlin. Springer, Hei-delberg, p. 211.
Lehmann, B., 2020. Formation of tin ore deposits: A reassessment. Lithos 105756.

Li, J., Huang, X.L., 2013. Mechanism of Ta–Nb enrichment and magmatic evolution in the Yashan granites, Jiangxi Province, south China. Acta Petrol. Sin. 29, 4311–4322 in Chinese with English abstract.
Li, J., Huang, X.L., He, P.L., Li, W.X., Yu, Y., Chen, L., 2015. In situ analyses of micas in the Yashan granite, South China: Constraints on magmatic and hydrothermal evolutions of W and Ta-Nb bearing granites. Ore Geol. Rev. 65, 793–810.
Li, J.K., Liu, S.B., Wang, D.H., Fu, X.F., 2007. Metallogenic epoch of Xuebaoding W-Sn-Be deposit in northwest Sichuan and its tectonic tracing significance. Mineral Depos. 26, 557–562 in Chinese with English abstract.
Liao, Y., Zhao, B., Zhang, D., Danyushevsky, L.V., Li, T., Wu, M., Liu, F., 2021. Evidence for temporal relationship between the late Mesozoic multistage Qianlishan granite complex and the Shizhuyuan W-Sn–Mo–Bi deposit, SE China. Sci. Rep. 11, 1–23.
Linnen, R.L., Lichtervelde, M.V., Černý, P., 2012. Granitic pegmatites as sources of strategic metals. Elements 8, 275–280.
Liu, Y., Deng, J., Li, C.F., Shi, G.H., Zheng, A.L., 2007a. REE composition in scheelite and scheelite Sm- Nd dating for the Xuebaoding W-Sn-Be deposit in Sichuan. Chin. Sci. Bull. 52, 2543–2550.
Liu, Y., Deng, J., Li, G., Shi, G., 2007b. Structure Refinement of Cs- rich and Na-Li Beryl and Analysis of Its Typomorphic Characteristic of Configurations. Acta Geol. Sin. 81, 61–67.
Liu, Y., Deng, J., Sun, D., Zhou, Y., 2007c. Morphology and Gensis Typomorphism of Minerals in W-Sn-Be Deposit of Huya, Sichuan. Editorial Committee Earth Sci.-J. China Univ. Geosci. 32, 75–81 in Chinese with English abstract.
Liu, Y., Deng, J., Zhang, G.B., Shi, G.H., Yang, L.Q., Wang, Q.F., 2010. $^{40}Ar/^{39}Ar$ Dating of Xuebaoding Granite in the Songpan-Garze Orogenic Belt, Southwest China, and its Geological Significance. Acta Geol. Sin. Engl. Ed. 84, 345–357.
Liu, Y., Deng, J., Shi, G., Sun, X., Yang, L., 2012a. Genesis of the Xuebaoding W-Sn-Be crystal deposits in southwest China: evidence from fluid inclusions, stable isotopes and ore elements. Resour. Geol. 62 (2), 159–173.
Liu, Y., Deng, J., Shi, G.H., Sun, D.S., 2012b. Geochemical and Morphological Characteristics of Coarse-grained Tabular Beryl from the Xuebaoding W-Sn-Be deposit, Sichuan Province, Western China. Int. Geol. Rev. 54 (14), 1673–1684.
Liu, H.G., Li, F., Zhang, X.L., 2018. Late Quaternary activity characteristics of Huya fault in the eastern margin of Qinghai Xizang Plateau. Earthq. Res. 41 (04), 594–604 in Chinese with English abstract.
Liu, C., Wang, R.C., Linnen, R.L., Wu, F.Y., Xie, L., Liu, X.C., 2023a. Continuous Be mineralization from two-mica granite to pegmatite: Critical element enrichment processes in a Himalayan leucogranite pluton. Am. Mineral. 108, 1.
Liu, X.C., Yu, P.P., Xiao, C.H., 2023b. Tin transport and cassiterite precipitation from hydrothermal fluids. Geosci. Front. 14, 101624 https://doi.org/10.1016/j.gsf.2023.101624.
London, D., 2008. Pegmatites. In: Martin, R.F. (Ed.), Canadian Mineralogist, 347 p. Special Publication 10.
London, D., 2015. Reading pegmatites: Part 1—What beryl says. Rocks Miner. 90, 138–153.
Macey, P., Harris, C., 2006. Stable isotope and fluid inclusion evidence for the origin of the Brandberg West area Sn-W vein deposits, NW Namibia. Miner. Deposita 41, 671–690.
Maniar, P.D., Piccoli, P.M., 1989. Tectonic discrimination of granitoids. Geol. Soc. Am. Bull. 101, 635–643.
Mao, J.W., Cheng, Y.B., Chen, M.H., Franco, P., 2013. Major types and time-space distribution of Mesozoic ore deposits in South China and their geodynamic settings. Miner. Deposita 48, 267–294.
Mao, J.W., Ouyang, H.G., Santosh, M., Yuan, S.D., Zhou, Z.H., Zheng, W., Liu, H., Liu, P., Chen, M.H., 2019. Geology and Metallogeny of Tungsten and Tin Deposits in China. SEG Special Publications 22, 411–482.
Middlemost, E.A.K., 1994. Naming materials in the magma igneous rock system. Earth Sci. Rev. 37, 215–224.
Miller, C.F., Miller, J.S., 2002. Contrasting stratified plutons exposed in tilt blocks, Eldorado Mountains, Colorado River Rift, NV, USA. Lithos 61, 209–224.
Miller, C.F., McDowell, S.M., Mapes, R.W., 2003. Hot and cold granites? Implications of zircon saturation temperatures and preservation of inheritance. Geology 31, 529–532.
Miller, C.F., Mittlefehldt, D.W., 1982. Depletion of light rare-earth elements in felsic magmas. Geology 10, 129–133.
Miller, C.F., Mittlefehldt, D.W., 1984. Extreme fractionation in felsic magma chambers: A product of liquid-state diffusion or fractional crystallization? Earth Planet. Sci. Lett. 68, 151–158.
Mlynarczyk, M.S.J., Williams-Jones, A.E., 2005. The role of collisional tectonic in the metallogeny of the Central Andean tin belt. Earth Planet. Sci. Lett. 240, 656–667.
Neiva, A.M.R., 2008. Geochemistry of cassiterite and wolframite from tin and tungsten quartz veins in Portugal. Ore Geol. Rev. 33, 221–238.
Pettke, T., Audetat, A., Schaltegger, U., Heinrich, C.A., 2005. Magmatic to hydrothermal crystallization in the W-Sn mineralized Mole Granite (NSW, Australia): Zone II: Evolving zircon and thorite trace element chemistry. Chem. Geol. 220, 191–213.
Rakovan, J.A., 2007. Word to Wise: Greisen. Rocks Miner. 82, 157–159.
Roberts, M.P., Clemens, J.D., 1993. Origin of High-Potassium, Calc-Alkaline. I-Type Granitoids. Geology 21 (9), 825–828.
Romer, R.L., Kroner, U., 2016. Phanerozoic tin and tungsten mineralization-Tectonic controls on the distribution of enriched protoliths and heat sources for crustal melting. Gondw. Res. 31, 60–95.
Simons, B., Andersen, J.C.Ø., Shail, R.K., Jenner, F.E., 2017. Fractionation of Li, Be, Ga, Nb, Ta, In, Sn, Sb, W and Bi in the peraluminous Early Permian Variscan granites of the Cornubian Batholith: Precursor processes to magmatic-hydrothermal mineralization. Lithos 278, 491–512.
Somarin, A.K., Ashley, A., 2004. Hydrothermal alteration and mineralization of the Glen Eden Mo-W-Sn deposit: a leucogranite-related hydrothermal system, Southern New England Orogen, NSW, Australia. Miner. Deposita 39, 282–300.
Sovacool, B.K., Ali, S.H., Bazilian, M., Radley, B., Nemery, B., Okatz, J., Mulvaney, D., 2020. Sustainable minerals and metals for a low-carbon future. Science 367, 30–33.
Tartèse, R., Boulvais, P., 2010. Differentiation of peraluminous leucogranites “en route” to the surface. Lithos 114, 353–368.
Taylor, J.R., Wall, V.J., 1993. Cassiterite solubility, tin speciation, and transport in a magmatic aqueous phase. Econ. Geol. 88, 437–460.
Trueman, D.L., Sabey, P., 2014. Beryllium. In: G. Gunn, Ed., Critical Metals Handbook. 99–119.
Wang, M., Deng, J., Hou, T., Derrey, I.T., Holtz, F., 2020. Experimental evidence for a protracted enrichment of tungsten in evolving granitic melts: implications for scheelite mineralization. Miner. Deposita 55 (4), 1299–1306.
Wang, P., Gray, T.P., Li, Z., Anderson, E.J.D., Allaz, J., Smyth, J.R., Koenig, A.E., Qi, L., Zhou, Y., Raschke, M.B., 2021. Mineralogical classification and crystal water characterisation of beryl from the W-Sn-Be occurrence of xuebaoding, sichuan province, western china. Mineral. Mag. 85 (2).
Whalen, J.B., Currie, K.L., Chappell, B.W., 1987. A-type granites: geochemical characteristics, discrimination and petrogenesis. Contrib. Miner. Petrol. 95, 407–419.
Wood, S.A., Samson, I.M., 2000. The hydrothermal geochemistry of tungsten in granitoid environments: I. Relative solubilities of ferberite and scheelite as a function of T, P, pH, and m NaCl. Econ. Geol. 95, 143–182.
Wu, F.Y., Jahn, B.M., Wilde, S.A., Lo, C.H., Yui, T.F., Lin, Q., Ge, W.C., Sun, D.Y., 2003a. Highly fractionated I-type granites in NE China (I): geochronology and petrogenesis. Lithos 66 (3–4), 241–273.
Wu, F.Y., Jahn, B.M., Wilde, S.A., Lo, C.H., Yui, T.F., Lin, Q., Ge, W.C., Sun, D.Y., 2003b. Highly fractionated I-type granites in NE China (II): isotopic geochemistry and implications for crustal growth in the Phanerozoic. Lithos 67 (3–4), 191–204.
Wu, F., Liu, X., Ji, W., Wang, J., Yang, L., 2017. Highly fractionated granites: Recognition and research. Sci. China Earth Sci. 60 (7), 1201–1219.
Xu, T., Li, Z.H., 2013. Characteristics of fluid inclusions and origin of ore-forming fluids in Xihuashan tungsten deposit, Jiangxi Province. Resour. Survey Environ. 34 (2), 95–101 in Chinese with English abstract.
Yan, D.P., Li, S.B., Cao, W.T., 2010. Multi layered and delamination crustal structure of Longmenshan: evidence of Neotectonic deformation and deep structure. Geosci. Front. 17 (5), 106–116 in Chinese with English abstract.
Ye, S., Qi, L., Luo, Y., Zhou, K., Pi, J., 2001. Realationship between the rare- metal contained granitic intrusions and beryl mineralization in Pingwu, Sichuan, China. Geol. Sci. Technol. Inform. 20, 65–70 in Chinese with English abstract.
Yokart, B., Barr, S.M., Williams-Jones, A.E., Macdonald, A.S., 2003. Late-stage alteration and tin-tungsten mineralization in the Khuntan Batholith, northern Thailand. J. Asian Earth Sci. 21, 999–1018.
Zhang, Y., Liu, Y., Zhu, X., Raschke, M.B., Shen, N., 2021. Genesis of highly fractionated granite and associated W-Sn-Be mineralization in the Xuebaoding area, Sichuan province, China. Ore Geol. Rev. 135 (3), 104197.
Zhang, D.L., Peng, J.T., Coulson, I.M., Hou, L.H., Li, S.J., 2014. Cassiterite U-Pb and muscovite 40Ar–39Ar age constraints on the timing of mineralization in the Xuebaoding Sn-W-Be deposit, western China. Ore Geol. Rev. 62, 315–322.
Zhao, P., Chu, X., Williams-Jones, A.E., Mao, J., Yuan, S., 2022. The role of phyllosilicate partial melting in segregating tungsten and tin deposits in W-Sn metallogenic provinces. Geology 50 (1).
Zhou, K.C., Qi, L.J., Xiang, C.J., 2002. Geological characteristics and gemological mineralization of beryl in Pingwu, Sichuan. Mineral Rock 4, 1–7 in Chinese with English abstract.
Zhu, X., Raschke, M.B., Liu, Y., 2020. Tourmaline as a Recorder of Ore-Forming Processes in the Xuebaoding W-Sn-Be Deposit, Sichuan Province, China: Evidence from the Chemical Composition of Tourmaline. Minerals 10 (5), 438.